Available online at www.sciencedirect.com
ScienceDirect
Cold Regions Science and Technology xx (2007) xxx – xxx
cold regions science and technology
www.elsevier.com/locate/coldregions

# Dense snow flowing past a deflecting obstacle: An experimental investigation

T. Faug *, M. Naaim, A. Fourriére

*UR ETNA, Cemagref Grenoble, BP 76, 38402 Saint-Martin d'Héres, France*

**Abstract**

Dense snow flowing down a rough inclined chute and interacting with a deflecting obstacle is experimentally investigated. These experiments are of considerable practical interest for the design of deflecting dams that are built to defend against large-scale snow avalanches. Our study focused on the maximum run-up reached by the dense flowing snow on a deflector. It was found that the maximum run-up was strongly correlated to the upstream Froude number and the deflecting angle of the obstacle. The data was compared with the predictions from a simple conversion of kinetic energy to potential energy on one hand and with oblique shock calculations on the other hand. The predicted values from the first approach were in better agreement with the measured values in comparison with the second approach. During a short transient phase at the end of the flow, it was shown that the flow features from our snow experiments were identical to the flow features from the previous granular and water experiments. In these conditions, the shallow-layer theory was also found to be relevant for snow flows.


*Keywords:* Avalanche dynamics; Snow; Deflecting dam; Experiments; Oblique shock; Maximum run-up

## 1. Introduction

One means of protecting mountainous areas against dense snow avalanches is to build passive defense structures in the run-out zone of the snow avalanche in order to divert, brake, and stop the avalanche. Design of defense structures is still based on empirical arguments. Many studies have been conducted over the last few years in order to analyze the effectiveness of different protection structures against snow avalanches. Several approaches have been used: (i) full-scale observations of snow avalanches interacting with defence structures (Larsen and Norem, 1996; Harbitz et al., 2000; Jóhannesson, 2001; Lied et al., 2002), (ii) small-scale laboratory experiments with granular flows (Chu et al., 1995; Hákonardóttir et al., 2001, 2003a; Faug et al., 2002, 2003, 2004a; Platzer et al., 2004), and, to a lesser extent, *in situ* chute experiments with snow flows (Hákonardóttir et al., 2003b), and (iii) numerical simulations (Naaim, 1998; Chiou et al., 2005). Other studies combined numerical simulations with full-scale terrain observations (Domaas and Harbitz, 1999; Harbitz et al., 2000) or laboratory experiments (Tai et al., 2001; Gray et al., 2003; Faug et al., 2004b; Naaim et al., 2003, 2004).

The problem of the interaction between a snow avalanche and a deflecting dam has been investigated by direct observations (Domaas and Harbitz, 1999; Jóhannesson, 2001), but there is still insufficient information in order to properly evaluate the effectiveness of such deflecting structures. Recent experimental investigations on high Froude number free surface flows

* Corresponding author. Tel.: +33 4 76 76 28 28; fax: +33 4 76 51 38 03.
*E-mail address:* thierry.faug@cemagref.fr (T. Faug).

0165-232X/$ - see front matter © 2007 Elsevier B.V. All rights reserved.
doi:10.1016/j.coldregions.2007.01.003

interacting with a deflector have been reported (Hákonardóttir and Hogg, 2005). The authors show that oblique shocks, observed for laboratory flows of water or of dry granular materials, are described well by shock equations in the framework of shallow-water theory, as has also been suggested by Gray et al. (2003).

The present paper deals with a series of *in situ* experiments (at the Lac Blanc pass in Alpe d'Huez, France) conducted with dense snow flows down an inclined chute interacting with a deflecting vertical wall. The experiments were conducted in an attempt to answer the following question: How does one estimate the maximum run-up reached by a dense snow flow on a deflecting obstacle?

The paper is organized as follows. Section 2 deals with theoretical approaches that can be used as an attempt to predict the maximum run-up reached by a dense snow flow on a deflector. The first attempt (Section 2.1) is simply based on the conversion of the kinetic energy to potential energy and is generally used for snow engineering applications (Salm, 1990; Jóhannesson, 2001). The second one (Section 2.2) comes from shock theory in the framework of shallow flows and was shown to be relevant for small-scale laboratory flows of granular materials and of water (Hákonardóttir and Hogg, 2005; Gray et al., 2003). We then describe the experimental set-up of the Lac Blanc pass (Section 3.1) and the main features of the incoming snow flows upstream of the deflection (Section 3.2) before analysing the deflected flow along the obstacle (Section 3.3). Section 4 is devoted to the comparison of the data in terms of maximum run-up along the obstacle with the predictions from the equations proposed in Section 2. We discuss the results in comparison with the results from small-scale laboratory flows of water or of dry granular materials.

## 2. Calculating the maximum run-up reached on a deflector

In this section we present two different ways to estimate the maximum run-up reached on the deflector: (i) the first one comes from simple conversion of kinetic energy to potential energy, and (ii) the second one is based on an oblique shock calculation.

### 2.1. Conversion of kinetic energy to potential energy

A naive estimate of the maximum run-up reached by the flowing material on the deflecting obstacle can be made by a simple conversion of kinetic energy to potential energy, assuming that the component of velocity normal to the obstacle vanished and is compensated by the increase in flow depth:

$$\frac{(u\sin\gamma)^2}{2} = g\Delta h\cos\theta, \tag{1}$$

where $\Delta h = h_{\max} - h$ is the increase in flow depth as illustrated in Fig. 1 along with the other variables in Eq. (1). In this formulation, it is assumed that no energy is lost during the impact of the snow particles with the obstacle, nor due to friction with the obstacle as the snow particles move along the obstacle after the impact. The equation leads to the following one:

$$\frac{h_{\max}}{h} = 1 + \frac{1}{2}(Fr^*\sin\gamma)^2, \tag{2}$$

where $Fr^* = \frac{u}{\sqrt{gh\cos\theta}}$. This formulation predicts that the maximum run-up should be correlated with the square of $Fr^*\sin\gamma$. Note that this formulation is generally used in snow engineering for dam design (Salm, 1990; Jóhannesson, 2001) but it doesn't take into account the formation of oblique shocks occurring when the incoming flow is supercritical (see Section 2.2).

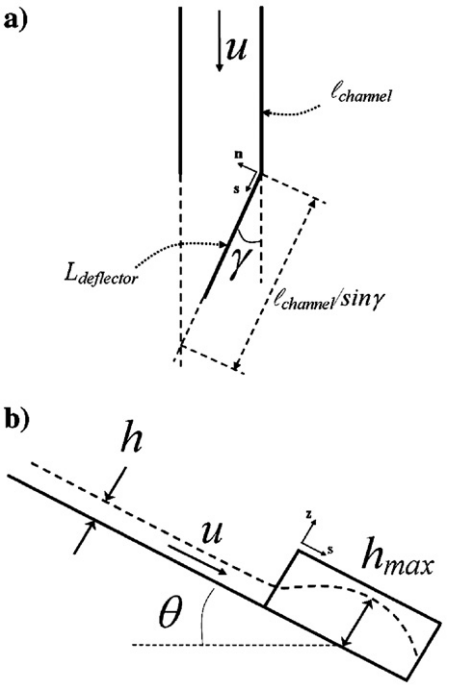


Fig. 1. Schematic diagrams of the deflector down a slope inclined at an angle $\theta$. (a) Plan view: the incoming speed of the flow is $u$ before interaction with the deflector positioned at an angle $\gamma$ to the flow direction. The channel width is $l_{\text{channel}}$ and the deflector length is $L_{\text{deflector}}$. (b) Side view: the maximum run-up reached by the flow on the deflector is $h_{\max}$.

Please cite this article as: Faug, T. et al. Dense snow flowing past a deflecting obstacle: An experimental investigation. Cold Reg. Sci. Technol. (2007), doi:10.1016/j.coldregions.2007.01.003

### 2.2. Oblique shocks

Normal and oblique shocks are usually discussed in gas dynamics. Some analogy to this was first discussed in water flows, where the name "hydraulic jump" was coined. Shocks in cohesionless granular material dynamics have been investigated more recently: normal granular shocks similar to the so-called hydraulic jumps in (Savage, 1979) and granular oblique shocks in (Rericha et al., 2002; Gray et al., 2003; Hákonardóttir and Hogg, 2005). These oblique shocks are described well by the so-called shock theory. Fig. 2 provides a schematic diagram of oblique shocks. Here in, $h_1$ and $\overrightarrow{u_1}$ are, respectively, the flow depth and the velocity upstream of the shock, $h_2$ and $\overrightarrow{u_2}$ are the flow depth and the velocity downstream of the shock, and $\beta$ is the shock angle. The motion upstream of the shock is parallel to the side walls of the chute so that $\overrightarrow{u_1} = (u_1, 0)$. The motion downstream of the shock is assumed to be tangential to the wall, so that the velocity $\overrightarrow{u_2}$ can be written as $\overrightarrow{u_2} = (u_2 \cos\gamma,\ u_2 \sin\gamma)$. The jump condition to conserve mass and momentum imply:

$$h_1 u_1 \sin\beta = h_2 u_2 \sin(\beta-\gamma) \tag{3}$$

$$\frac{1}{2} g \cos\theta h_1^2 + h_1 u_1^2 \sin^2\beta = \frac{1}{2} g \cos\theta h_2^2 + h_2 u_2^2 \sin^2(\beta-\gamma) \tag{4}$$

$$h_1 u_1^2 \sin\beta\cos\beta = h_2 u_2^2 \sin(\beta-\gamma)\cos(\beta-\gamma) \tag{5}$$

These equations can be solved to give the depth ratio $h_2/h_1$ as a function of the upstream Froude number $Fr_1^* = \frac{u_1}{\sqrt{g h_1 \cos\theta}}$ and the shock angle $\beta$:

$$\frac{h_2}{h_1} = \frac{1}{2}\left(\sqrt{1 + 8(Fr_1^* \sin\beta)^2} - 1\right) \tag{6}$$

Note that it may be possible to include a source term in equations as an attempt to catch features of flows that accelerate (Gray et al., 2003). Here we only present the equations without including source terms. The study from Hákonardóttir and Hogg (2005) showed that these equations work well to describe steady oblique shocks occurring with high Froude number flows of water and of dry granular material. Note that ones can define an implicit equation between the shock angle $\beta$, the incoming Froude number $Fr_1^*$ and the deflecting angle $\gamma$ (see Hákonardóttir and Hogg (2005)):

$$\tan\gamma = \frac{4 \sin\beta \cos\beta (1 - Fr_1^{*2} \sin^2\beta)}{-3 + 4\cos^2\beta - 4\cos^2\beta Fr_1^{*2} - \sqrt{1 + 8 Fr_1^{*2} \sin^2\beta}} \tag{7}$$

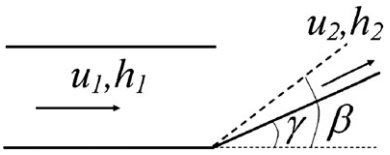


Fig. 2. The oblique shock configuration when we consider the deflection of a uniform and steady downslope flow with velocity $u_1$ and depth $h_1$ by a rigid barrier orientated at an angle $\gamma$ to the incoming flow direction. $\beta$ is the shock angle, $u_2$ and $h_2$ are the velocity and the depth of the flow downstream of the shock.

## 3. Experimental set-up and main qualitative data

### 3.1. Description of the experimental set-up

The experimental device we used is an intermediate scale device built at the Lac Blanc pass, near the Alpe d'Huez ski resort in the French Alps. It consists of a flow chute that can be artificially fed with snow through a hopper. The chute is 10 m long and 0.20 m wide. The bottom of the chute is lined with rough sandpaper. The channel has been instrumented to measure flow depth, normal and shear stresses at the bottom, and the velocity profile within the flow. Through variations in chute inclination and feeding rate, access to a wide range of slopes and flow depths is available. Fig. 3 shows the device (more details can be found in (Bouchet et al., 2003)). In winter 2004–2005, the device was fitted with an inclined plane, located at the end of the channel, on which a deflecting obstacle was set-up. The flow in the inclined plane was free on one side and constrained by the deflecting obstacle on the other side. It corresponded to the typical configuration of a snow avalanche interacting with a deflecting dam (Jóhannesson, 2001) except that our experiments involved a vertical deflecting wall. The effect of the upstream slope of the deflector (fixed at 90° in our experiments) is therefore not discussed in this paper. The same configuration with a vertical deflecting wall was used in the laboratory experiments described by Hákonardóttir and Hogg (2005). As illustrated in Fig. 3, two video cameras provided the means to study the interaction between the obstacle and the flow: video camera 0 showed the modifications of the free surface in the vicinity of the obstacle (side view) and video camera 1 analyzed the flow spreading downstream

Please cite this article as: Faug, T. et al. Dense snow flowing past a deflecting obstacle: An experimental investigation. Cold Reg. Sci. Technol. (2007), doi:10.1016/j.coldregions.2007.01.003

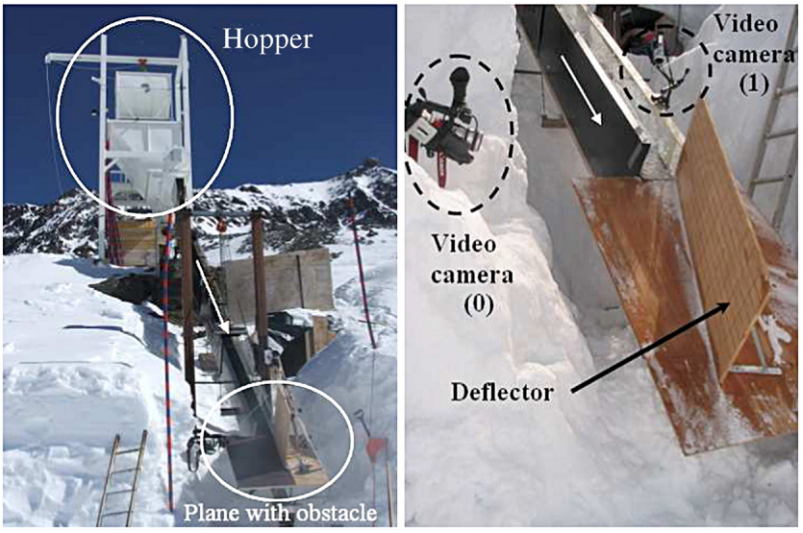


Fig. 3. Experimental set-up: view of the channel with the inclined plane and the deflecting obstacle (left) and detailed view of the deflecting obstacle (right). Two video cameras were installed to study the mean features of the flow interacting with the deflecting obstacle.

from the deviation (top view). The deflector was made out of wood. A grid was drawn on its surface in order to measure the maximum run-up of snow on the obstacle.

The parameters of the system, which could be varied, were: (i) the feeding mass flow rate, (ii) the chute inclination $\theta$, and (iii) and the deflecting angle of the obstacle $\gamma$. The slope of the plane at the end of the chute was equal to the chute inclination $\theta$.

### 3.2. Features of the flow upstream of the obstacle

The experimental device provides steady and uniform snow flows as described in (Bouchet et al., 2003, 2004). Systematic measurements of the velocity profiles for different chute inclinations showed the existence of a typical velocity profile with two zones of different shearing: a thin high-shear zone surmounted by a weak sheared zone. The velocity profile has not yet been theoretically described, but it seems to be explained by the existence of clusters due to cohesion (Rognon et al., 2005). The velocity profile is fixed by the channel inclination, the feeding mass flow rate, and the roughness at the base. The velocity profile provides the means to calculate the mean velocity $u$. The reference upstream snow flow is then characterized by its Froude number $Fr = \frac{u}{\sqrt{gh}}$, where $h$ is the flow depth.

Four series of measurements (23/02/2005, 02/03/2005, 16/03/2005, 31/03/2005) were conducted during the winter 2005, but the video camera 0 did not function during the third series of measurements (16/03/2005).The basal surface of the plane was smooth (wood) for the first experiments (23/02/2005). The plane was covered with the same roughness as the bottom of the chute for the following experiments (02/03/2005, 16/03/2005, 31/03/2005). The length of the deflector was 0.70 m.

Three series of measurements (25/01/2006, 31/01/2006, 26/04/2006) were taken during the winter 2006. The basal surface of the plane was smooth (wood) for all the experiments in winter 2006. The length of the deflector was increased and equal to 1.40 m.

All the experiments, except the last series in winter 2006 (26/04/2006), were conducted during the night in order to guarantee the use of dry snow (no liquid water), the snow was made up of fine snow grains (weak cohesion) and the air and snow temperatures were negative (see Table 1). The last series of winter 2006 (26/04/2006) was made during the morning with sun light and involved humid fresh snow. This last series did not allow observation of the interaction of the flow with the deflector because the snow was not able to flow down until the end of the channel.

The Froude number $Fr^*$ of the flows studied are given in Table 1 and ranged typically from 3 to 8. Depending on the incoming Froude number and the deflecting angle of the obstacle, that was varied from 0° to 18.5° in our experiments, the maximum run-up $h_{max}$ reached on the obstacle could be 3 times higher than the incoming flow depth. The Section 3.3 presents the mean features of the deflected flow.

Please cite this article as: Faug, T. et al. Dense snow flowing past a deflecting obstacle: An experimental investigation. Cold Reg. Sci. Technol. (2007), doi:10.1016/j.coldregions.2007.01.003

Table 1
Features of the reference flow: chute inclination $\theta$, velocity $u$, depth $h$, Froude number $Fr^* = u/\sqrt{gh\cos\theta}$, deflecting angle of the obstacle $\gamma$, air temperature $T_a$, snow temperature $T_s$

| Date | Flow | $\theta$ (°) | $u$ (ms$^{-1}$) | $h$ (cm) | $Fr^*$ | $\gamma$ (°) | $T_a$ (°C) | $T_s$ (°C) |
|---|---|---|---|---|---|---|---|---|
| 23/02/2005 | 1 | 38.0 | 4.30 | 9.9 | 4.9 | 0 | −18 | −18 |
| 23/02/2005 | 2 | 38.0 | 4.30 | 9.5 | 5.0 | 11.5 | −18 | −18 |
| 23/02/2005 | 3 | 39.5 | 4.70 | 9.4 | 5.6 | 18.5 | −18 | −18 |
| 23/02/2005 | 4 | 37.0 | 4.00 | 10.2 | 4.5 | 18.5 | −18 | −18 |
| 02/03/2005 | 5 | 41.0 | 4.45 | 8.6 | 5.6 | 5 | −19 | −21 |
| 02/03/2005 | 6 | 39.5 | 4.25 | 8.5 | 5.3 | 5 | −19 | −21 |
| 02/03/2005 | 7 | 38.0 | 4.00 | 9.2 | 4.7 | 5 | −19 | −21 |
| 02/03/2005 | 8 | 37.0 | 3.95 | 10 | 4.5 | 5 | −19 | −21 |
| 31/03/2005 | 15 | 39.5 | 4.10 | 10.1 | 4.7 | 0 | −3.3 | −6.7 |
| 31/03/2005 | 16 | 39.5 | 4.10 | 11.4 | 4.4 | 3.9 | −3.3 | −6.7 |
| 31/03/2005 | 17 | 39.5 | 4.10 | 11.2 | 4.4 | 8.9 | −3.3 | −6.7 |
| 31/03/2005 | 18 | 39.5 | 4.10 | 11.8 | 4.3 | 13.8 | −3.3 | −6.7 |
| 25/01/2006 | 19 | 37.0 | 3.77 | 8.0 | 4.8 | 2.5 | −13 | −17 |
| 25/01/2006 | 20 | 37.0 | 4.14 | 10.8 | 4.5 | 5 | −13 | −17 |
| 25/01/2006 | 22 | 37.0 | 3.84 | 8.2 | 4.8 | 7.5 | −13 | −17 |
| 25/01/2006 | 23 | 35.5 | 3.49 | 8.7 | 4.2 | 7.5 | −13 | −17 |
| 25/01/2006 | 24 | 35.5 | 2.93 | 4.8 | 4.7 | 7.5 | −13 | −17 |
| 25/01/2006 | 26 | 35.5 | 3.74 | 11.4 | 3.9 | 10 | −13 | −17 |
| 25/01/2006 | 29 | 34.5 | 3.38 | 11.9 | 3.4 | 10 | −13 | −17 |
| 31/01/2006 | 30 | 39.5 | 4.75 | 8.2 | 6.0 | 10 | −5.9 | −7.4 |
| 31/01/2006 | 31 | 39.5 | 4.52 | 6.5 | 6.5 | 10 | −5.9 | −7.4 |
| 31/01/2006 | 33 | 39.5 | 4.78 | 9.1 | 5.7 | 15 | −5.9 | −7.4 |
| 31/01/2006 | 34 | 38.0 | 4.10 | 3.8 | 7.4 | 10 | −5.9 | −7.4 |
| 31/01/2006 | 35 | 38.0 | 4.70 | 9.0 | 5.6 | 15 | −5.9 | −7.4 |
| 31/01/2006 | 36 | 38.0 | 4.48 | 6.1 | 6.5 | 15 | −5.9 | −7.4 |

The second column gives the number of the flow. $h$ is the flow depth at the location $s=0$ (end of the channel). The basal surface of the plane was rough (sandpaper) for flows 5–18 and smooth for flows 1–4 and flows 19–36 (wood).

### 3.3. Analysis of the influence of the deflecting obstacle

The changes in flow depth versus time at a given location $s$ were displayed with the films obtained from video camera 0. Fig. 4 shows an example (flow 3 in Table 1: $\theta=39.5°$ and $\gamma=18.5°$) how the flow depth evolved over time at two different locations of the obstacle ($s=0$ and $s=0.5$ m). We observed three phases: (i) a transient phase when the front of the snow flow interacted with the obstacle, (ii) the stationary phase, and (iii) the transient phase when the flow came to rest. No splash-up, as described in (Hákonardóttir and Hogg, 2005) was observed during the front and obstacle interaction. The films from both video cameras showed that there was a progressive increase in flow depth along the obstacle before reaching a steady state.

As can be seen in Fig. 4, we observe the height had periodic fluctuations, as was observed for the upstream flow in the channel (Bouchet et al., 2003, 2004). The maxima of these variations traveled with the flow. Bouchet et al. (2003, 2004) suggested that these variations are not waves intrinsic to the flow but are due to the feeding system. The flow depth $h(s)$ at location $s$ was calculated as follows: $h(s)=\int_{t_1}^{t_2} z(s)\mathrm{d}t$, where $t_1$ and $t_2$ corresponded to the beginning and the end of the stationary phase, respectively. The value of $h$ given in Table 1 corresponded to the position $s=0$. Calculating $h(s)$, $s$ ranging from 0 – end of the channel – to 0.70 m (winter 2005) or 1.40 m (winter 2006) — end of the obstacle, gave the height of the free surface along the obstacle.

The qualitative analysis of the films from video camera 0 brought out the following points: the height reached on the obstacle increased when the Froude number and the deflecting angle of the obstacle increased. We defined the maximum run-up $h_{max}$ reached on the obstacle as it is defined in Fig. 5 (side view from camera 0). This maximum run-up was generally well defined except for a few cases for which the deflecting angle of the obstacle and the Froude number were both high (flows 3 and 18 in table 1). Indeed, in these cases, the maximum run-up did not seem to be reached before the end of the obstacle, which was probably not long enough. That is why the length of the deflector was increased from 0.70 m to 1.40 m during the winter 2006. Note that the direction of the downstream flow is parallel to the deflector as can be seen in Fig. 5 (top view from camera 1).

The observations showed that the maximum run-up reached on the deflector mainly depended on the upstream Froude number and the deflecting angle of the obstacle. The maximum steady run-up $h_{max}$, normalized by the upstream reference flow depth $h$, was quantified

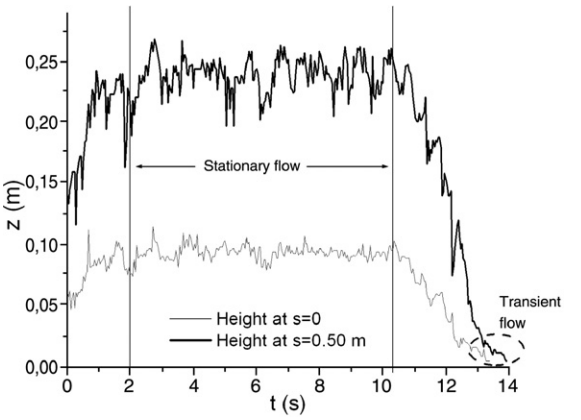


Fig. 4. Flow depth versus time for two different locations along the dam: $s=0$ and $s=0.5$ m. Example for $\theta=39.5°$, $\gamma=18.5°$, $L_{deflector}=0.70$ m (winter 2005, flow 3).

Please cite this article as: Faug, T. et al. Dense snow flowing past a deflecting obstacle: An experimental investigation. Cold Reg. Sci. Technol. (2007), doi:10.1016/j.coldregions.2007.01.003

according to the Froude number and the deflecting angle of the channel:

$$\frac{h_{max}}{h} = \frac{h_{max}}{h}(Fr^*, \gamma) \quad (8)$$

The maximum run-up reached on the obstacle during this stationary phase is compared to predictions from theoretical approaches in Section 4.1.

## 4. Maximum run-up on the deflecting obstacle

### 4.1. Steady flows

In this section we only consider the steady phase of the snow flows experiments (see the stationary phase in Fig. 4). Fig. 6 shows the variation of the maximum run-up (normalized by the upstream flow depth) reached on the obstacle versus the upstream Froude number for different deflecting angles of the obstacle. The maximum run-up increased when the Froude number increased. If we compare the case with a low deflecting angle ($\gamma = 5°$) and the case with a higher deflecting angle ($\gamma = 18.5°$), the maximum run-up was greater when the deflecting angle was higher for a fixed Froude number. Only a small range of Froude numbers was investigated, but the results indicate the qualitative trend.

Fig. 7 shows the variation of the maximum run-up (normalized by the reference flow depth) versus the

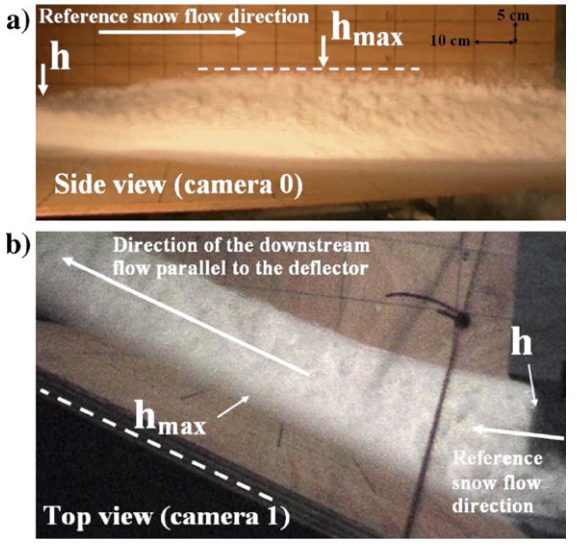


Fig. 5. a) camera 0, upstream photo: side view of the maximum run-up on the dam. Example for $\theta = 38°$ and $\gamma = 15°$ (flow 36, winter 2006); b) camera 1: downstream photo: top view of the deflected flow. The direction of the downstream flow is parallel to the deflector. Example for $\theta = 37°$ and $\gamma = 18.5°$ (flow 4, winter 2005).

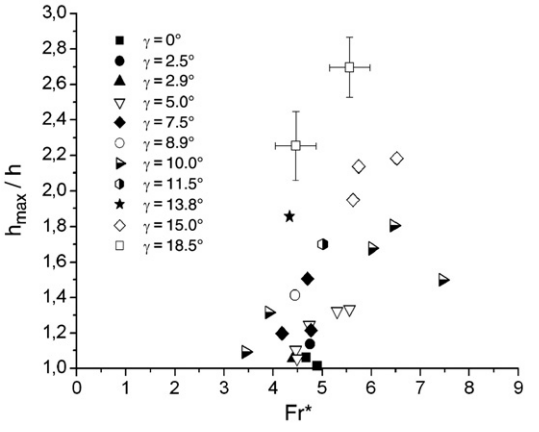


Fig. 6. Normalized maximum run-up versus the Froude number for different angles of the deflecting obstacle. The typical error bars correspond to the standard deviation due to the height fluctuations (see Fig. 4).

deflecting angle of the obstacle for different ranges of Froude numbers. The maximum run-up increased substantially when the deflecting angle of the obstacle increased. The maximum run-up was approximately three times higher than the incoming flow depth for a deflecting angle of 18.5° and an incoming Froude number of about 6.

Some typical depth profiles along the obstacle are given in Fig. 8. Here we plotted the dimensionless height of the flow along the deflector ($z/h$) as a function of the dimensionless distance along the deflector ($s/h$). Also plotted are the predictions of the steady depth from both (i) a simple conversion of kinetic energy to potential energy (Eq. (2)) and (ii) the shock conditions (Eq. (6)). The results show that a simple conversion of kinetic energy to potential energy gives a good estimation of the maximum run-up whereas a shock calculation tends to over-estimate the maximum run-up that is observed from experiments.

In Fig. 9, the experimentally measured dimensionless maximum run-up is compared with the theoretically calculated values, which are derived from Eqs. (2) and (6). The data in Fig. 9 comprise all the experimental series listed in Table 1. We note that there seems to be a better agreement of the experimental measurements with the predictions from simple conversion of kinetic energy to potential energy (Eq. (2)) than with ones from the shock conditions (Eq. (6)). These results are now discussed in details.

The studies from Hákonardóttir and Hogg (2005) and Gray et al. (2003) dealing with dry granular flows show that shock calculations are very relevant to predict the depth of the flow at the deflecting obstacle,

Please cite this article as: Faug, T. et al. Dense snow flowing past a deflecting obstacle: An experimental investigation. Cold Reg. Sci. Technol. (2007), doi:10.1016/j.coldregions.2007.01.003

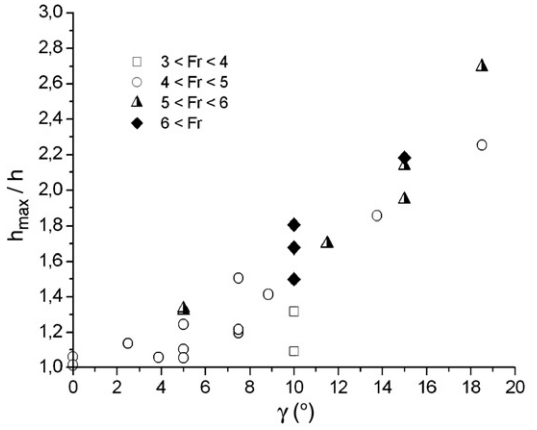


Fig. 7. Normalized maximum run-up versus the deflecting angle of the obstacle for different ranges of the incoming Froude number. We did not mention here the error bars that are similar the error bars shown in Fig. 6.

downstream of the shock, relative to the upstream depth (see Fig. 6 in (Hákonardóttir and Hogg, 2005)). To explain that our results are not in contradiction with the conclusions from Hákonardóttir and Hogg (2005) and Gray et al. (2003), we have to consider the main differences between the experimental conditions. In our experiments the incoming flow is thick. The flow depth $h$ is typically equal to 10 cm, leading to a ratio $h/l_{\text{channel}} \approx 1/2$ (where $l_{\text{channel}}$ is the width of the channel) whereas Hákonardóttir and Hogg studied granular flows that were characterized by a ratio $h/l_{\text{channel}}$ typically equal to 1/50. The granular flows that they studied can be considered as shallow flows, which is confirmed by the good agreement between their experiments and the shallow-layer theory whereas our snow flows are far from being shallow flows during the stationary phase ($h/l_{\text{channel}} \approx 1/2$).

Furthermore note that Hákonardóttir and Hogg showed the existence of a transition zone that corresponds to the initial spatial development of the oblique shock. Hence the deflecting obstacle has to be long enough in order to see the shock. In their experiments the length of this transition zone is typically between 20 and 50 times the flow depth. In our experiments the ratio $L_{\text{deflector}}/h$ is typically between 7 (winter 2005) and 14 (winter 2006) for a given incoming flow depth around 10 cm. Therefore we might think that we can only see the initial development of the shock towards the steady and uniform state shock depth. However, our experiments show that the predictions from the shock calculation are always higher than the measured maximum run-up for all the series which would correspond to the transition zone (see Fig. 8). This result seems to be a different result from Fig. 8 in (Hákonardóttir and Hogg, 2005). Keeping our incoming flow conditions (ratio $h/l_{\text{channel}} \approx 1/2$) and increasing the length of the deflector would not increase the maximum run-up and the depth profile along the deflector because the flow was supercritical. Moreover the comparison of the results from winter 2005 and 2006 where the length of the deflector was increased by a factor 2 showed that the depth profile was not influenced by the length of the deflector. Therefore, in these conditions we think that the shock calculation would fail in predicting the uniform and steady state flow depth. The analysis of the experiments showed that a simple conversion of kinetic energy to potential energy seems to be sufficient to

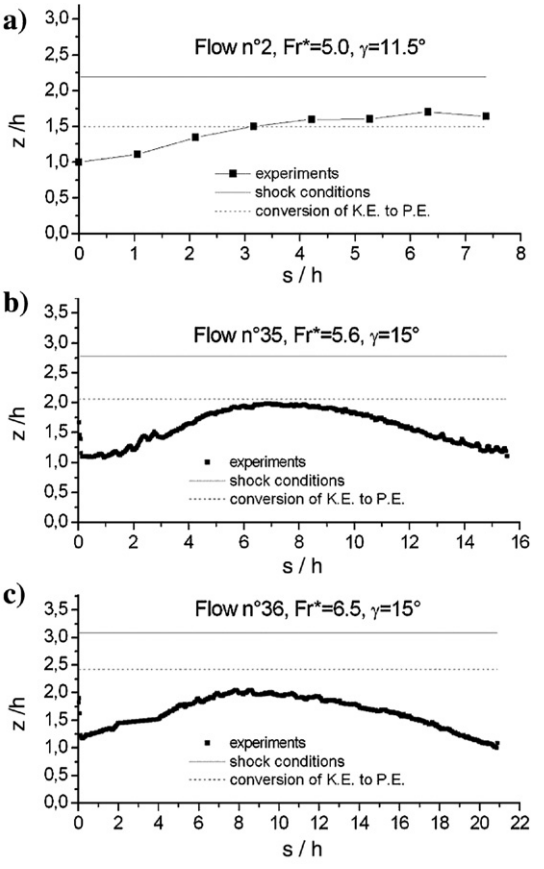


Fig. 8. The dimensionless height of the flow along the obstacle, $z/h$, as a function of the dimensionless distance along the dam, $s/h$, for (a) flow 2 with $Fr^*=5.0$, $\gamma=11.5°$, $r_1=L_{\text{deflector}}/h=7$ and $r_2=L_{\text{channel}}/(h \sin \gamma)=10$, (b) flow 35 with $Fr^*=5.6$, $\gamma=15°$, $r_1=14$ and $r_2=7.8$, (c) flow 36 with $Fr^*=6.5$, $\gamma=15°$, $r_1=14$ and $r_2=7.8$. Also plotted are the predictions from conversion of kinetic energy K.E. to potential energy P.E. (dashed line) and of shock calculations (solid line). For comparison with Eq. (6), the shock $\beta$ angle was calculated from the implicit equation between $Fr^*$, $\gamma$ and $\beta$ as is mentioned at the end of the Section 2.2 in Eq. (7).

Please cite this article as: Faug, T. et al. Dense snow flowing past a deflecting obstacle: An experimental investigation. Cold Reg. Sci. Technol. (2007), doi:10.1016/j.coldregions.2007.01.003

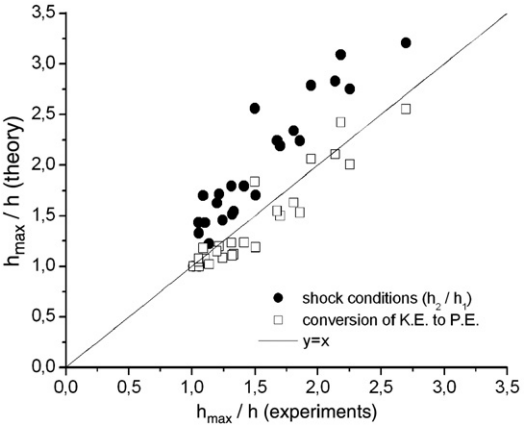


Fig. 9. Predicted values of the dimensionless maximum depth reached along the dam from simple conversion of kinetic energy to potential energy (Eq. (2), white squares) and from shock calculations (Eq. (6), black circles) versus the measured ones. For comparison with Eq. (6), the shock angle $\beta$ was calculated from the implicit equation between $Fr*$, $\gamma$ and $\beta$ as is mentioned at the end of the Section 2.2.

predict the measured values of the maximum run-up in the range of the following values of the Froude number $Fr*$ and the deflecting angle $\gamma$: $3<Fr*<8$ and $0<\gamma<18.5°$. In addition to the ratio $L_{\text{deflector}}/h$, it's crucial to consider the ratio $l_{\text{channel}}/(h \sin \gamma)$. With a ratio $h/l_{\text{channel}} \approx 1/2$ and with values of the deflecting angle $\gamma$ ranging from 5 to 20°, the ratio $l_{\text{channel}}/(h \sin \gamma)$ typically ranged between 6 and 46 in our snow experiments. In the granular flows tests, with a ratio $h/l_{\text{channel}} \approx 1/50$ and with values of the deflecting angle $\gamma$ ranging from 8 to 32° (Hákonardóttir and Hogg, 2005), the ratio $l_{\text{channel}}/(h \sin \gamma)$ typically ranged between 95 and 360. To our opinion the main argument to explain our observations and results is the fact that the incoming flow was far from being a shallow flow. If the snow chute had been wider (and the dam longer) — or if the flow had been thinner, we would have observed shocks well predicted by the shock theory in the framework of shallow flows. These conditions occurred during a short transient phase at the end of the flow when the flow became thinner: we observed transient snow oblique shocks very similar to those observed with granular flows, as it is described in the following section. Note that we also defined the ratio $r = \frac{L_{\text{deflector}}}{(l_{\text{channel}}/\sin\gamma)}$ which indicated if the dam extended out the incoming flow ($r>1$) or not ($r<1$) as illustrated in Fig. 1. In our snow chute experiments the ratio $r$ ranged from 0.15 to 1.1 (winter 2005) and from 0.3 to 2.2 (winter 2006). In the granular flows tests from Hákonardóttir and Hogg (2005), the ratio $r$ ranged from 0.3 to 1. Then the values of the ratio $r$ were very similar for our snow chute experiments and the granular flows tests.

### 4.2. Transient flows

In this section we consider the transient phase of the snow flows experiments (see Fig. 4). At the end of the flow when the flow became very shallow and only if the basal roughness of the plan was smooth, we could observe snow jumps very similar to those observed by Hákonardóttir and Hogg. During this short duration phase, the flow was very shallow. The upstream flow depth was typically equal to 1 cm, leading to a ratio $h/l_{\text{channel}} \approx 1/20$ and $L_{\text{deflector}}/h \approx 70$ (for $L_{\text{deflector}}=70$ cm) and $L_{\text{deflector}}/h \approx 140$ (for $L_{\text{deflector}}=140$ cm). Then the ratio $l_{\text{channel}}/(h \sin \gamma)$ defined in the previous section ranged from 60 to 460. These values correspond to the typical values that were considered in (Hákonardóttir and Hogg, 2005). Fig. 10 shows an example of the snow oblique shocks that we observed (flow 4 in Table 1: $\gamma=18.5°$, $\theta=37°$ and a smooth surface at the base). The side view (from camera 0) illustrates the high $h_2/h_1$ depth ratio in this case. The top view (camera 1) illustrates the shock angle $\beta$ as defined in the dry granular dynamics literature. Fig. 11 displays the experimental depth ratio $h_2/h_1$ according to the upstream Froude number $Fr_1^*$ that we estimated in our experiments (flow 4 in Table 1) in comparison with Eq. (6). The downstream flow depth $h_2$ was precisely measured but we could only roughly

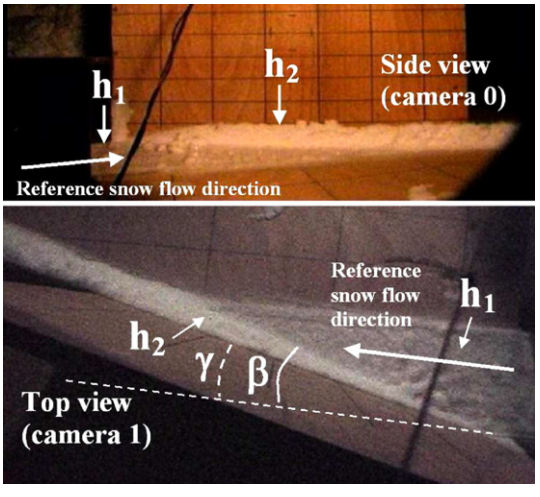


Fig. 10. Snow jump: side view of the oblique shock (camera 0: upstream photo) and top view of the oblique shock (camera 1: downstream photo). We reported the deflecting angle of the obstacle $\gamma$ and the shock angle $\beta$ as defined in (Gray et al., 2003; Hákonardóttir and Hogg, 2005). Example for $\theta=37°$ and $\gamma=18.5°$ (winter 2005, flow 4).

Please cite this article as: Faug, T. et al. Dense snow flowing past a deflecting obstacle: An experimental investigation. Cold Reg. Sci. Technol. (2007), doi:10.1016/j.coldregions.2007.01.003

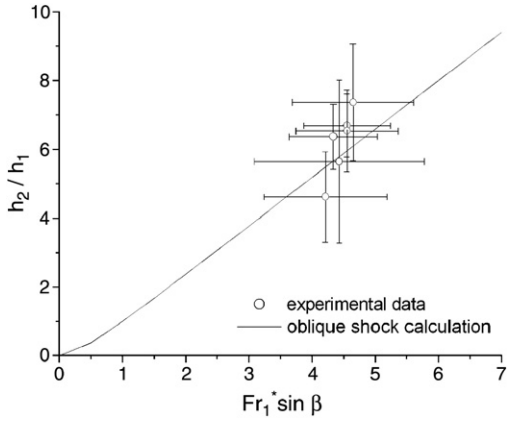


Fig. 11. Snow oblique shock (flow 4): $h_2/h_1$ versus $Fr_1^*$ sin $\beta$, where $h_1$ and $h_2$ are the flow depth upstream and downstream of the jump, $Fr_1^*$ is the upstream Froude number and $\beta$ is the oblique shock angle.

estimate the incoming flow depth $h_1$ (the flow depth and its fluctuations were on the same order during this phase), explaining the high values of error bars displayed in Fig. 11. In spite of these high values of the error bars, good agreement was found between the experimental data and Eq. (6). The velocity was estimated using small insulated clusters at the surface of the flow, as shown in Fig. 10. The velocity was found to be close to the measured velocity during the stationary phase, i.e., roughly 4 m $s^{-1}$.

This led to local upstream Froude numbers typically 13. In the dry granular dynamics literature (Gray et al., 2003; Hákonardóttir and Hogg, 2005), similar oblique shocks described as sudden are observed for granular flows with a high upstream Froude number above 5. Gray et al. (2003) did study granular jumps with Froude numbers less than five and described these shocks as diffuse. In our experiments with snow, we observed sudden oblique shocks for high upstream Froude number values (10–15). Note that these values were therefore much higher than those measured during the stationary phase (3–8).

## 5. Concluding remarks and discussion

The experimental set-up allowed analysing the interaction of a steady snow flow with a deflector. The experimental features of the experiments were characterized by the following parameters: the incoming Froude number $Fr^*$, the deflecting angle of the obstacle $\gamma$, the ratio of the deflector length to the flow depth $L_{\text{deflector}}/h$ and the ratio $\frac{l_{\text{channel}}}{h\sin\gamma}$ (involving the ratio of the flow depth to the channel width $h/l_{\text{channel}}$). The typical values of the snow flows that we studied during the steady phase were the following ones: $Fr^*$ ranged from 3 to 8, $\gamma$ ranged from 0 to 18.5°, $L_{\text{deflector}}/h \approx 10$ and $h/l_{\text{channel}} \approx 1/2$. In these conditions it was not possible to observe a sudden oblique shock but the deflected flow reached a maximum run-up that could be well characterized and predicted by a simple conversion of kinetic energy to potential energy. Shock calculations were also used as an attempt to match the measured values without luck (the predicted values are higher than the measured ones). During a short transient phase at the end of the flow, the flow became very shallow and the values of the governing parameters changed as follows: $Fr^* \approx 13$, $L_{\text{deflector}}/h \approx 100$ and $h/l_{\text{channel}} \approx 1/20$. Then transient oblique shocks were observed with similar features as the steady shocks observed with water and granular materials (Hákonardóttir and Hogg, 2005).

A future challenge would be to build a wider channel to investigate the occurrence of oblique snow shocks in steady conditions. Further detailed investigations using experiments and numerical computations are needed to study many of the effects involved in natural situations that could improve the predictions: (i) the effect of source terms, including gravity and basal friction (rheology of the material, bed roughness) and (ii) the effect of the shape of the obstacle. The progress of these investigations would be of a crucial practical interest for the design of protection dams to deflect dangerous snow avalanches.

## Acknowledgements

The authors thank Hervé Bellot, Frédéric Ousset, Pierre Rognon, Xavier Ravanat, Chloé Bois who helped conduct experiments at the Lac Blanc pass. This work received financial support from the European Union within the SATSIE EUFP5 project. The authors are very grateful to K.M. Hákonardóttir and T. Jóhannesson for fruitful discussions that allowed improving the paper.

## References

Bouchet, A., Naaim, M., Ousset, F., Bellot, H., Cauvard, D., 2003. Experimental determination of constitutive equations for dense and dry avalanches: presentation of the set-up and first results. Surv. Geophys. 24 (5–6), 525–541.

Bouchet, A., Naaim, M., Bellot, H., Ousset, F., 2004. Experimental study of dense snow avalanches: velocity profiles in steady and fully developed flows. Ann. Glaciol. 38, 30–34.

Chiou, M.C., Wang, Y., Hutter, K., 2005. Influence of obstacles on rapid granular flows. Acta Mech. 175, 105–122.

Chu, T., Hill, G., McClung, D.M., Ngun, R., Sherkat, R., 1995. Experiments on granular flows to predict avalanche runup. Can. Geotech. J. 32, 285–295.

Please cite this article as: Faug, T. et al. Dense snow flowing past a deflecting obstacle: An experimental investigation. Cold Reg. Sci. Technol. (2007), doi:10.1016/j.coldregions.2007.01.003

Domaas, U., Harbitz, C.B., 1999. On avalanche run-up heights on deflecting dams: centre-of-mass computations compared to observations. NGI publication. 203, report 581210-4.

Faug, T., Lachamp, P., Naaim, M., 2002. Experimental investigation on steady granular flows interacting with an obstacle down an inclined channel: study of the dead zone upstream from the obstacle. Nat. Hazards Earth Syst. Sci. 2 (3/4), 187–191.

Faug, T., Naaim, M., Bertrand, D., Lachamp, P., Naaim-Bouvet, F., 2003. Varying dam height to shorten the run-out of dense avalanche flows: developing a scaling law from laboratory experiments. Surv. Geophys. 24 (5–6), 555–568.

Faug, T., Naaim, M., Naaim-Bouvet, F., 2004a. An equation for spreading length, centre of mass and maximum run-outs shortenings of avalanche flows by obstacle. Cold Reg. Sci. Technol. 39 (2/3), 141–151.

Faug, T., Naaim, M., Naaim-Bouvet, F., 2004b. Experimental and numerical study of granular flow and fence interaction. Ann. Glaciol. 38, 135–138.

Gray, J.M.N.T., Tai, Y.C., Noelle, S., 2003. Shock waves, dead zones and particle free regions in rapid granular free surface flows. J. Fluid Mech. 491, 160–181.

Hákonardóttir, K.M., Hogg, A.J., 2005. Oblique shocks in rapid granular flows. Phys. Fluids 17, 077101.

Hákonardóttir, K.M., Jóhannesson, T., Tiefenbacher, F., Kern, M., 2001. A laboratory study of the retarding effect of breaking mounds in 3, 6 and 9 m long chutes. Technical report. Vedurstofa Islands. Report No. 01007.

Hákonardóttir, K.M., Hogg, A.J., Jóhannesson, T., Tómasson, G.G., 2003a. A laboratory study of the retarding effects of braking mounds on snow avalanches. J. Glaciol. 49 (165), 191–200.

Hákonardóttir, K.M., Hogg, A.J., Jóhannesson, T., Kern, M., Tiefenbacher, F., 2003b. Large-scale avalanche braking mound and catching dam experiments with snow: a study of the airborne jet. Surv. Geophys. 24 (5–6), 543–554.

Harbitz, C.B., Domaas, U., Engen, A., 2000. Design of snow avalanche deflecting dams. Internationales Symposium, Interpraevent 2000, Villach, Osterreich, vol. 1. Tagunspublikation, pp. 383–396.

Jóhannesson, T., 2001. Run-up of the two avalanches on the deflecting dams at Flateyri, northwestern Iceland. Ann. Glaciol. 32, 350–354.

Larsen, J.O., Norem, H., 1996. The effect of dam constructions as mitigative measures. 14 years of experience from a full-scale project. International conference “avalanches and related subjects”, Proceedings. Kirovsk, Russie, pp. 59–65. 2–6-september 1996.

Lied, K., Moe, A., Kristensen, K., Issler, D., 2002. Full scale avalanche test site and the effect of the catching dam. NGI report 581200-35. Norwegian Geotechnical Institute.

Naaim, M., 1998. Dense avalanche numerical modeling, interaction between avalanche and structures. In Hestnes, E., Ed. 25 Years of snow Avalanche Research, Voss 12–16- May 1998, Proceedings, Oslo, NGI Publications 203, 187–191.

Naaim, M., Faug, T., Naaim-Bouvet, F., 2003. Dry granular flow: erosion and deposition modelling. Surv. Geophys. 24 (5–6), 569–585.

Naaim, M., Naaim-Bouvet, F., Faug, T., Bouchet, A., 2004. Dense snow avalanche modeling: flow, erosion, deposition and obstacle effects. Cold Reg. Sci. Technol. 39 (2/3), 193–204.

Platzer, K.M., Margreth, S., Bartelt, P., 2004. Granular flow experiments to investigate dynamic avalanche forces for snow shed design. In: Bartelt, V., Adam, Christen, Sack, Sato (Eds.), Snow engineering. Taylor and Francis Group, London.

Rericha, E.C., Bizon, C., Shattuck, M.D., Swinney, H.L., 2002. Shocks in supersonic sand. Phys. Rev. Lett. 88, 014302.

Rognon, P.G., Roux, J.-N., Chevoir, F., Naaim, M., 2005. Dense flows of bidisperse assemblies of disks down an inclined plane. In: Garcia-Rojo, Herrmann, Mc Namara (Eds.), Powders and grains. ISBN: 0 415 38348 X, pp. 795–798.

Salm, B., 1990. Schnee, Lawinen und Lawinenschutz. Lecture notes. ETH Zurich. Abt. II, VI, VIII, X.

Savage, S.B., 1979. Gravity flow of cohesionless granular materials in chutes and channels. J. Fluid Mech. 92, 53–96.

Tai, Y.C., Gray, J.M.N.T., Hutter, K., Noelle, S., 2001. Flow of dense avalanches past obstructions. Ann. Glaciol. 32, 281–284.

Please cite this article as: Faug, T. et al. Dense snow flowing past a deflecting obstacle: An experimental investigation. Cold Reg. Sci. Technol. (2007), doi:10.1016/j.coldregions.2007.01.003